Gas-Phase Collisional Relaxation of the CH_2I Radical after UV Photolysis of CH_2I_2

Thomas Lenzer, Kawon Oum,* Jörg Schroeder,* and Kentaro Sekiguchi

Institut für Physikalische Chemie, Universität Göttingen, Tammannstrasse 6, D-37077 Göttingen, Germany

Received: July 6, 2005; In Final Form: October 4, 2005

Transient UV absorption spectra and kinetics of the CH_2I radical in the gas phase have been investigated at 313 K. Following laser photolysis of 1−3 mbar CH_2I_2 at 308 nm, transient spectra in the wavelength range 330−390 nm were measured at delay times between 60 ns and a few microseconds. The change of the absorption spectra at early times was attributed to vibrational cooling of highly excited CH_2I radicals by collisional energy transfer to CH_2I_2 molecules. From transient absorption decays measured at specific wavelengths, time-dependent concentrations of vibrationally "hot" and "cold" CH_2I and CH_2I_2 were extracted by kinetic modeling. In addition, the transient absorption spectrum of CH_2I^* radicals between 330 and 400 nm was reconstructed from the simulated concentration−time profiles. The evolution of the absorption spectra of CH_2I^* radicals and $CH_2I_2^*$ due to collisional energy transfer was simulated in the framework of a modified Sulzer−Wieland model. Additional master equation simulations for the collisional deactivation of CH_2I^* by CH_2I_2 yield $\langle\Delta E\rangle$ values in reasonable agreement with earlier direct studies on the collisional relaxation of other systems. In addition, the simulations show that the shape of the vibrational population distribution of the hot CH_2I^* radicals has no influence on the measured UV absorption signals. The implications of our results with respect to spectral assignments in recent ultrafast spectrokinetic studies of the photolysis of CH_2I_2 in dense fluids are discussed.

1. Introduction

For more than 30 years, the photodissociation dynamics of diiodomethane in the ultraviolet has been the subject of considerable experimental and theoretical interest. This is largely due to the complexity of the electronically excited states of CH_2I_2 that give rise to a complicated photodissociation pattern. It is well-known that the broad UV absorption spectrum of CH_2I_2 is the result of overlapping transitions to several excited states.[1−3] It may be represented, for example, by Gaussian bands centered at 209, 249, 288, and 312 nm, which, according to Kawasaki, arise from at least five electronic transitions to excited states ($2A_1$, $1A_1$, B_2, $2B_1$, and $1B_1$) which correlate with different photodissociation channels. It is well established that photolysis in the UV near 300 nm leads to direct C−I bond dissociation with overall unity quantum yield via channels 1a and 1b:[4−6]

$$CH_2I_2 + h\nu \rightarrow CH_2I + I\,(^2P_{3/2}) \qquad (1a)$$

$$\rightarrow CH_2I + I^*\,(^2P_{1/2}) \qquad (1b)$$

The branching ratios into different dissociation channels have been measured at various excitation wavelengths. The quantum yield of excited iodine atoms (I*) is generally less than 0.5,[4,7] and Baughcum and Leone estimated the branching ratio of channel 1a/channel 1b to be ∼3:1 after photolysis at 308 nm.[3] Most of the available excess excitation energy remains as internal energy in the methyleneiodide product radical.[8] About 80% of the available energy after photolysis at 308 nm appears as vibrational and rotational excitation of the CH_2I radical, adding up to an internal energy of ∼13 000 cm^{-1} for channel 1a and ∼5400 cm^{-1} for channel 1b.[3,9] In fact, recent ion imaging studies by Xu et al. present a more refined view.[9] Following up on earlier studies of Kroger et al.[2] and Jung et al.,[10] who found a much broader translational energy distribution for channel 1a compared to channel 1b, they could resolve two major dissociation channels in the formation of $I(^2P_{3/2})$ via process 1a. They also confirmed that $I^*(^2P_{1/2})$ in process 1b is mainly produced by one dominant dissociation channel.[9] The resulting initial distribution of internally "hot" CH_2I radicals in our experiments, produced by excitation at 308 nm, will therefore be trimodal, with an average energy of roughly 10 300 cm^{-1}.

The nascent hot CH_2I radicals ("CH_2I^*") subsequently undergo collisional energy transfer with CH_2I_2 (in the absence of other bath gas molecules):

$$CH_2I^* + CH_2I_2 \rightarrow \rightarrow \rightarrow CH_2I + CH_2I_2^* \qquad k_2 \quad (2)$$

Comparing with other studies on collisional energy transfer, one would expect the absorption spectrum of the methyleneiodide radical to change with time, exhibiting a rather broad band initially after photodissociation which should narrow as the radical cools due to vibrational relaxation.[11] So far, the time evolution of the CH_2I^* radical absorption spectrum neither has been quantitatively measured nor has been taken into account in transient absorption studies of the CH_2I_2 photodissociation. Only a "cold" CH_2I radical gas-phase spectrum in the UV region is available from the work of Sehested et al., which was reconstructed from a set of time-resolved absorption profiles recorded at different wavelengths.[12]

Information on the temporal evolution of the nascent CH_2I^* absorption spectrum is of particular interest in conjunction with recent femtosecond laser experiments on the photoinduced dynamics of CH_2I_2 in the condensed phase, where the assignment of observed spectral transients in the near UV to visible

* To whom correspondence should be addressed. E-mail: koum@gwdg.de (K.O.); jschroe2@gwdg.de (J.S.). Phone: +49 551 39 12598. Fax: +49 551 39 3150.

10.1021/jp053686w CCC: $30.25
Published on Web 11/12/2005

region is still controversial.[13−16] Cooling of vibrationally highly excited intermediates and products is thought to be a key process in the photoinduced isomerization of CH_2I_2 observed in liquids and supercritical fluids.[16−18] One aim of the current study is therefore to shed some light on the spectral evolution of CH_2I^* to obtain information on its collisional energy transfer behavior.

In the gas phase, Baughcum and Leone studied collisional energy transfer of CH_2I^* using IR emission spectroscopy.[3] Assuming the average energy transferred per collision for $CH_2I^* + CH_2I_2$ to be constant with $\langle \Delta E \rangle = -1900$ or -1250 cm^{-1}, depending on the formation of CH_2I^* from channel 1a or 1b, respectively, the authors estimated a quenching rate constant of $k_2 = (1-5) \times 10^{-11}$ cm^3 molecule^{-1} s^{-1}. Note that recent comparisons of such IR emission measurements with results from more accurate experiments employing "kinetically controlled selective ionization (KCSI)" by Lenzer, Luther, and coworkers show that uncertainties by up to a factor of 5 are not unusual in emission measurements of collisional energy transfer, because of considerable uncertainties in the calibration curve relating the IR emission intensity to the internal energy of the molecule.[19]

In the absence of an additional bath gas, one also has to consider the subsequent cooling of vibrationally excited $CH_2I_2^*$ generated in process 2 due to collisions with the parent molecule

$$CH_2I_2^* + CH_2I_2 \rightarrow \rightarrow \rightarrow 2CH_2I_2 \qquad k_3 \qquad (3)$$

which was estimated to be ~10 times slower than the collisional relaxation of the CH_2I radical.[3] Baughcum and Leone's vibrational cooling rate constants are probably a useful estimate at high energies and possibly an upper limit to the true value at lower energies, as cooling rates are expected to slow with decreasing excess energy, resulting in smaller values for k_2 or k_3 after a few collisions.[20]

In liquid and supercritical solution, the vibrational relaxation of CH_2I_2 was studied following excitation of C−H-stretch overtone and combination bands, as pioneered by Crim and coworkers and later on also investigated by other groups[21−26] at fairly low internal excess energies of CH_2I_2 up to 6000 cm^{-1}. The relaxation rates, as expected, strongly depend on the properties of the solvent molecules (they range from several hundred picoseconds in supercritical xenon to below 20 ps in $(CD_3)_2CO$), and a straightforward comparison with gas-phase values for binary collisions with the parent molecule CH_2I_2 is not possible. This is also complicated by the high CH_2I_2/collider ratio applied in the condensed-phase experiments,[22,23] resulting in contributions of both CH_2I_2 + collider and $CH_2I_2 + CH_2I_2$ collisions to the observed relaxation rates.

Our current study of CH_2I^* radicals photolytically generated from CH_2I_2 has the goal of providing reliable estimates of the energy transfer behavior of these two species and their energy-dependent absorption cross sections between 330 and 400 nm. These data will hopefully prove useful for the interpretation of time-resolved femtosecond pump−probe experiments on CH_2I_2 photolysis in this spectral region and future studies of related systems.

2. Experimental Section

Gas-phase CH_2I radicals were generated by excimer laser photolysis of CH_2I_2 at 308 nm in a temperature-controlled optical cell (path length, 60 cm; optical diameter, 3 cm). The laser beam was unfocused and operating at less than 10^5 W/cm^2 in order to avoid possible multiphoton processes such as the sequential dissociation $CH_2I_2 \rightarrow CH_2I \rightarrow CH_2$.[2,3] The typical pressure of the precursor CH_2I_2 was 1−3 mbar, with degrees of excitation varying between 1 and 10%. Time-resolved transient UV absorption spectra were recorded from 330 to 390 nm between 60 ns and 6 μs using a spectrograph (resolution, 0.1 nm; slit width, 120 μm) coupled to an ICCD camera (minimum gating time, 50 ns). A high-pressure xenon arc lamp was used as the light source. A pulse/delay generator controlled the timing between the laser system and the ICCD data acquisition system. Prior to obtaining the transient spectrum, a reference spectrum was measured without the laser beam under the same experimental conditions. Several hundred spectra were usually averaged. Kinetic traces at distinct wavelengths between 330 and 400 nm were detected by a prism-monochromator photomultiplier arrangement with a bandwidth of 2 nm and recorded using a digital storage oscilloscope. Typically, several hundred shots were averaged, which allowed the progress of reaction 1 to be monitored. CH_2I_2 (Aldrich, 99%) was used as received and thoroughly degassed in several freeze−pump−thaw cycles prior to use.

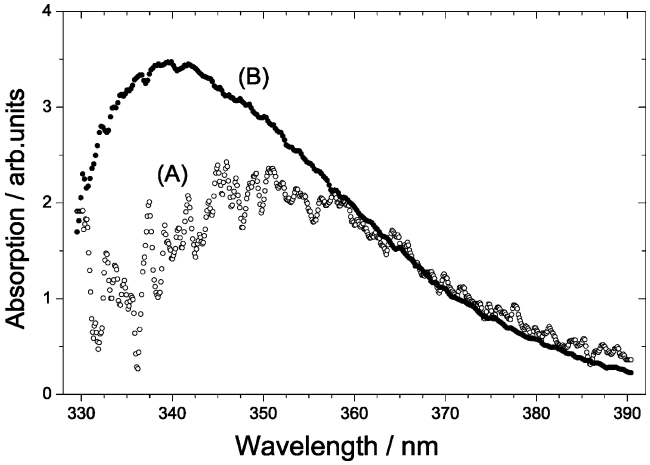

Figure 1. Transient absorption spectra recorded after 308 nm photolysis of CH_2I_2 at 313 K. Open circles: curve A, $p(CH_2I_2) = 1.3$ mbar, averaged over 60−110 ns. Filled circles: curve B, $p(CH_2I_2) = 3$ mbar, averaged over 1−6 μs.

3. Results and Discussion

3.1. Transient UV Absorption Spectra after Photolysis of CH_2I_2 in the Gas Phase. Our aim was to record transient absorption spectra of CH_2I radicals at particular delay times after photolysis, and to relate these to the respective internal energy of the CH_2I^* radical. Following laser photolysis of CH_2I_2 at 308 nm, we averaged transient spectra in the wavelength range 330−390 nm under different experimental conditions. Two examples are shown in Figure 1: Curve A was obtained at an initial pressure of 1.3 mbar CH_2I_2 over a time range of 60−110 ns (detecting CH_2I^* radicals after about a single collision with CH_2I_2), whereas curve B was recorded at 3 mbar CH_2I_2 over 1−6 μs (after ~120 collisions). The hard-sphere-type collision number was estimated by using the diameters 5.7 and 4.3 Å for CH_2I_2 and CH_2I, respectively.[3]

First, we discuss spectrum A in Figure 1. The absorption is most intense at ~350 nm and decreases monotonically toward longer wavelengths. The sharp drop of the absorption signal below 340 nm is caused by the depletion of the precursor due to photolysis. At a delay time of 110 ns after photolysis of 1.3 mbar CH_2I_2, the CH_2I^* radical is expected to have experienced on average only a single collision with parent CH_2I_2. Using the energy-independent average energy transferred per collision $\langle \Delta E \rangle = -1900$ cm^{-1} for $CH_2I^* + CH_2I_2$, as given by Leone,[3]

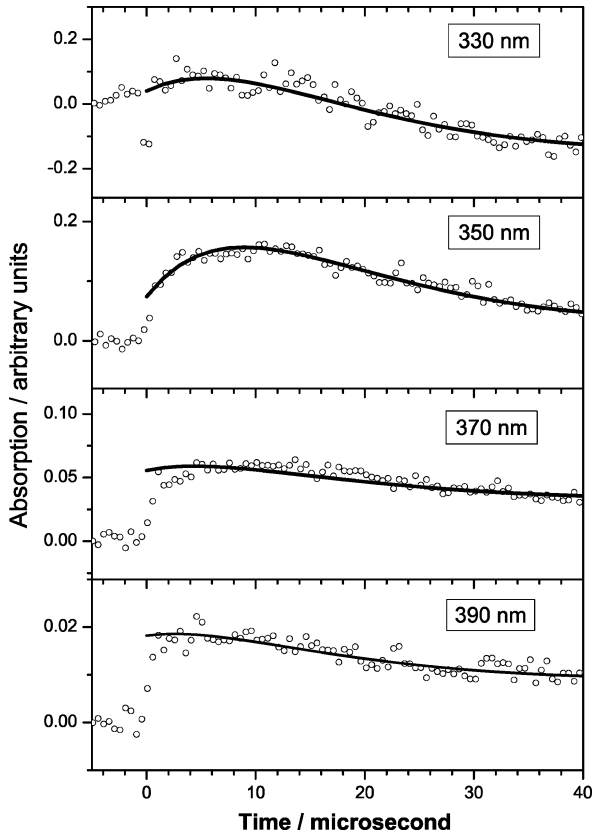

Figure 2. Absorption signals at different wavelengths recorded after photolysis of CH_2I_2 ($p(CH_2I_2) = 1.3$ mbar, $T = 313$ K; signal averaged over 100 laser shots). Open circles, experimental data; thick solid lines, total absorption signal from the kinetic modeling (see text).

one would estimate that CH_2I^* has lost roughly 1900 cm^{-1} of internal energy after 110 ns, leaving the CH_2I^* with an internal energy of ~8500 cm^{-1}. This corresponds to an estimated vibrational temperature of ~3000 K (employing the canonical partition function for CH_2I with normal-mode frequencies taken from the work of Zhang et al.: 3174, 1353, 609, 166, 3335, and 855 cm^{-1}).[8] However, as will be shown below, the $\langle \Delta E \rangle$ values in this regime deduced from our present study are much smaller, around −800 cm^{-1}, so that CH_2I^* is left with approximately 9600 cm^{-1} after a single collision (~3200 K). Given this temperature, we believe that curve A is a combination of an absorption component from CH_2I^* radicals and a bleaching component from the initial decrease of the CH_2I_2 concentration on photolysis.

In contrast to curve A in Figure 1, curve B was recorded with a higher initial concentration of CH_2I_2 and averaged over a longer delay range at later times. In the presence of 3 mbar CH_2I_2, excited CH_2I^* radicals have experienced ~120 collisions with CH_2I_2 by a delay time of 6 μs. On the basis of our master equation simulations (see section 3.4), we believe that absorption B represents already a cold CH_2I spectrum with additional contributions from heated $CH_2I_2^*$. We will consider this in a more detailed analysis below.

3.2. CH_2I Radical Kinetics Following CH_2I_2 Photolysis in the Gas Phase. To estimate the individual contributions of different species to the measured transient absorption spectrum, we analyzed the relaxation kinetics of CH_2I^* radicals with CH_2I_2 at different wavelengths. Figure 2 shows a representative set of transient absorption signals at several UV probe wavelengths following photolysis of 1.3 mbar CH_2I_2 at 313 K. Typical concentrations in Figure 2 were $[CH_2I_2]_0 = (3-6) \times 10^{16}$ molecule cm^{-3} and $[CH_2I^*]_0 = (0.3-3) \times 10^{15}$ molecule cm^{-3}. As it turns out, major contributions to the total absorption signal up to ~30 μs arise from the concentration changes of CH_2I^* and $CH_2I_2^*$ via relaxation processes 2 and 3. On the other hand, as the vibrational relaxation of CH_2I^* radicals has already proceeded considerably, the subsequent loss of CH_2I radicals takes place in the time range ~15−50 μs under our conditions. The subsequent reactions considered in our model are reactions with the precursor molecule CH_2I_2 (4), self-combination (5), and reactions with I atoms (6) and I_2 (7):[6,7,12,27]

$$CH_2I + CH_2I_2 \rightarrow CH_2I{-}CH_2I + I \qquad \Delta H_r = -172 \text{ kJ mol}^{-1} \quad (4a)$$

$$\rightarrow C_2H_4 + I_2 + I \qquad \Delta H_r = -130 \text{ kJ mol}^{-1} \quad (4b)$$

$$CH_2I + CH_2I\ (+M) \rightarrow CH_2I{-}CH_2I\ (+M) \qquad \Delta H_r = -387 \text{ kJ mol}^{-1} \quad (5a)$$

$$\rightarrow C_2H_4 + I_2 \qquad \Delta H_r = -115 \text{ kJ mol}^{-1} \quad (5b)$$

$$CH_2I + I\ (+M) \rightarrow CH_2I_2\ (+M) \qquad \Delta H_r = -214 \text{ kJ mol}^{-1} \quad (6)$$

$$CH_2I + I_2 \rightarrow CH_2I_2 + I \qquad \Delta H_r = -64 \text{ kJ mol}^{-1} \quad (7)$$

In the presence of excess CH_2I_2 (relative to CH_2I or I) and a total pressure of 1−3 mbar, reaction 4 represents the major loss channel for cold CH_2I radicals, and reactions 5−7 do not play an important role. Furthermore, the absorption cross section of $CH_2I{-}CH_2I$ is too small to account for any significant contribution to the total absorption signal.[28] The rate constant k_4 is unfortunately not known and used as a fitting parameter in our kinetic model: a value of $k_4 \approx 3 \times 10^{-12}$ cm^3 $molecule^{-1}$ s^{-1} was optimized. Thermodynamic data were taken from the earlier work of Furuyama et al.[29,30] The radial diffusion loss was a minor channel under our experimental conditions with an estimated rate smaller than 10^3 s^{-1}. While a complete modeling with a detailed sensitivity analysis of these processes up to 100 μs is possible in a complete reaction scheme, we restrict the discussion in this paper to the dynamics at early times.

The initial absorption change within the first few microseconds is dominated by spectral changes induced by vibrational cooling of CH_2I^* radicals and the concomitant heating of CH_2I_2 due to energy transfer process 2. Because the concentration of the parent molecule CH_2I_2 is in excess compared to those of photolytic products, process 2 is considered to be the fastest under our experimental conditions and will govern the dynamics at early times, before subsequent reactions will play a larger role. In the present kinetic modeling, CH_2I and CH_2I^* (as well as CH_2I_2 and $CH_2I_2^*$) are treated as "individual" species, and keeping the condition $[CH_2I]_{total} = [CH_2I] + [CH_2I^*]$. At this stage, we introduce this simplification in the kinetic analysis, because it is not necessary to consider the detailed change of vibrational population distributions and temperature-dependent absorption cross sections, $\sigma(CH_2I^*,T)$, in the kinetic modeling. This strategy is also supported by our master equation simulations discussed in section 3.4. The error ranges of $\sigma(CH_2I^*,T)$ from the kinetic fitting procedure reflect the uncertainty of the values due to this simplification of assuming a fixed vibrational

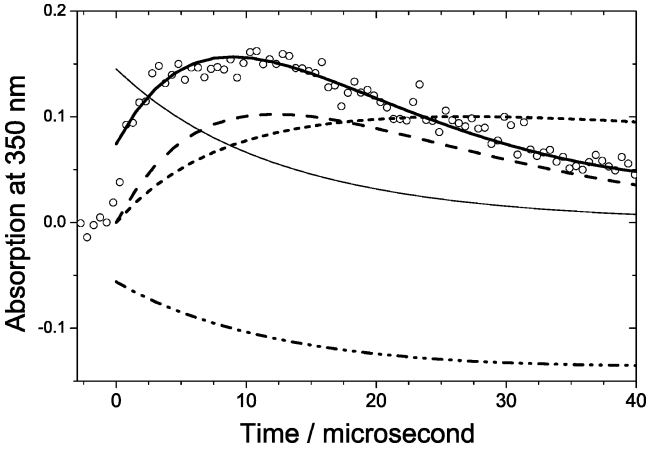

Figure 3. Detailed kinetic modeling result for the absorption signal at 350 nm recorded after photolysis of CH_2I_2 ($p(CH_2I_2) = 1.3$ mbar, $T = 313$ K; signal averaged over 100 laser shots). Open circles, experimental data; thick solid curve, simulated total absorption signal from the kinetic modeling (see text); thin solid curve, fitted profile of CH_2I^*; dashed curve, fitted profile of CH_2I; dash−dot−dotted curve, fitted profile of CH_2I_2; short-dashed curve, fitted profile of $CH_2I_2^*$.

temperature for the excited and cold species. As far as $CH_2I_2^*$ in processes 2 and 3 is concerned, its time-dependent vibrational temperature is not exactly known. However, for the estimation of $\sigma(CH_2I_2^*,T)$, the shock wave experimental data over the temperature range from 300 to 1400 K of Henning et al.[31] are available. Therefore, prior to the kinetic fitting procedure, we could estimate the temperature-dependent $\sigma(CH_2I_2^*,T)$ using a modified Sulzer−Wieland model, the details of which are described in the next section. In the simplified description of collisional processes within our kinetic scheme, we used $\sigma(CH_2I_2^*,T)$ at a temperature around 1000 K as a starting value, which was allowed to vary within the range between 300 and 2500 K during the fitting process (see Figure 4A). The $\sigma(CH_2I_2^*)$ value obtained this way will be influenced by the simultaneous heating of CH_2I_2 and cooling of $CH_2I_2^*$ during the collision cascade via processes 2 and 3, respectively. In the simplified kinetic model, we obtained vibrational temperatures of $CH_2I_2^*$ between 1000 and 1400 K at the different wavelengths shown in Figure 2. The uncertainties of this range of the vibrational temperature and the $\sigma(CH_2I_2^*)$ value are reflected in the total error range of $\sigma(CH_2I^*)$ (see below).

With careful systematic modeling, it was possible to reproduce experimental time traces at different wavelengths, and the simulation results are plotted in Figure 2 as thick solid lines. Fitted time profiles of individual species, CH_2I^*, CH_2I, $CH_2I_2^*$, and CH_2I_2 were obtained, and an example at $\lambda = 350$ nm is plotted in Figure 3. We estimated the initial radical concentration assuming $[CH_2I^*]_0 \approx [CH_2I_2]_{consumed}$ due to photolysis of CH_2I_2, given the value of the absorption cross section, $\sigma(CH_2I_2)$, and the optical path length of 60 cm: this is reflected in the simulation result of the absorption signal of CH_2I_2 (see the dash−dot−dotted curve in Figure 3). We used a minimum set of fitting parameters including λ-dependent values of $\sigma(CH_2I^*)$ and $\sigma(CH_2I)$ as well as λ-independent values of k_2-k_4. The resulting values of absorption coefficients, σ, of CH_2I^* and CH_2I are plotted in Figure 4B. It is interesting to note that slower quenching rate constants of reactions 2 and 3 ($k_2 \approx 4 \times 10^{-12}$ and $k_3 \approx 4 \times 10^{-13}$ cm^3 molecule^{-1} s^{-1}) than those reported by Baughcum and Leone[3] were needed to fit the experimental data, although the ratio k_2/k_3 is similar. The sensitivity analysis indicates that the time traces of Figure 2 are sensitive to the parameters $\sigma(CH_2I^*)$, $\sigma(CH_2I)$, and $\sigma(CH_2I_2^*)$. The uncertainty

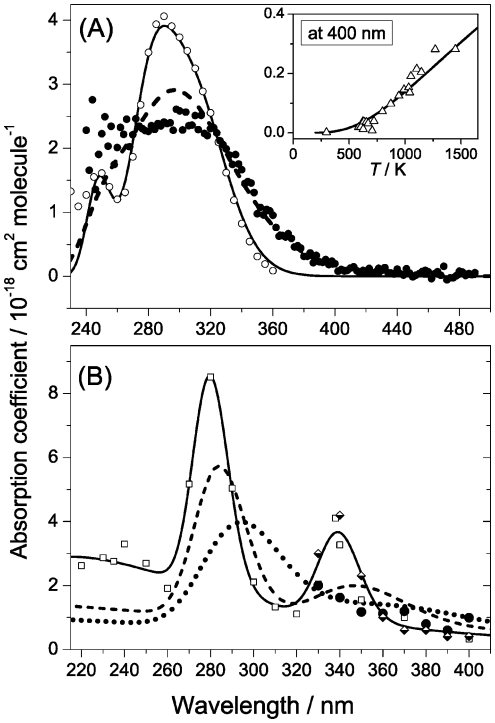

Figure 4. Simulations of the temperature dependence of the absorption cross sections using a modified Sulzer−Wieland formalism: (A) For CH_2I_2. Solid line simulation, at 300 K; dashed line simulation, at 1400 K. The experimental data at 300 K (open circles) and at 1400 K (filled circles) are from refs 31 and 22, respectively. Inset: the open triangles are experimental data for $\sigma(CH_2I_2)$ at 400 nm as a function of temperature from ref 22; the solid line is the simulation result from this work. (B) For CH_2I. Solid, dashed, and dotted line simulations at 300, 1500, and 3400 K, respectively. The experimental absorption cross sections of CH_2I^* at ~3400 K (filled circles) and CH_2I at 313 K (half-filled diamonds) were obtained from the kinetic model (see text); open squares, data from ref 12.

of the $\sigma(CH_2I_2^*)$ values is well-determined because of our Sulzer−Wieland fit to the experimental data. Moreover, for $\sigma(CH_2I)$, there is one previous measurement of $\sigma(CH_2I)$ in the literature which we could compare with our values as a reference: Sehested et al.[12] previously obtained a UV absorption spectrum of CH_2I radicals in the gas phase in a similar way as we did in Figure 4B. In their study, CH_2I radicals were generated via a fast reaction of F atoms with CH_3I following a microwave discharge in SF_6. They could observe only cold CH_2I radicals at 1 bar SF_6, as is expected at such an elevated pressure. Their transient CH_2I radical spectrum was determined from the maximum transient absorbance of time traces at distinct wavelengths in the range 220−400 nm and compares well with our spectrum in Figure 4B. In summary, considering not only the scatter of data but also including estimated systematic errors and the influence of the error range of $\sigma(CH_2I_2^*)$, we estimate the error ranges in our $\sigma(CH_2I^*)$ values in Figure 4B to be ~20−30% of their values.

3.3. Temperature-Dependent Absorption Coefficients, σ, of CH_2I_2 and CH_2I. In the course of the kinetic modeling described in section 3.2, the details of the temperature-dependent absorption coefficient of CH_2I_2 were required to simulate the contribution from $CH_2I_2^*$ forming and disappearing in the collisional energy transfer processes 2 and 3. We employed a modified Sulzer−Wieland model to estimate the temperature dependence of the spectra.[11,32−35] The absorption coefficient of quasi-diatomic molecules for a transition from a bound electronic ground state to a repulsive excited electronic state is given by

$$\sigma(\nu,T) = \sigma_{max}\frac{\nu}{\nu_0}\sqrt{\tanh\left(\frac{\theta_0}{2T}\right)}\exp\left\{-\tanh\left(\frac{\theta_0}{2T}\right)\left(\frac{\nu-\nu_0}{\Delta\nu_0}\right)^2\right\} \quad (8)$$

Here, σ_{max} is the maximum absorption coefficient, ν is the observation frequency, ν_0 is the absorption maximum at 0 K, $\Delta\nu_0$ is the half-width at half-maximum of the electronic spectrum at 0 K, T is the temperature of the sample, and $\theta_0 = hc\omega_0/k_B$ is the characteristic temperature of the vibration with wavenumber ω_0.[34] Astholz et al. successfully extended this simulation method to polyatomic systems such as substituted cycloheptatrienes, toluene, *p*-xylene, benzyl radicals, and methyl−benzyl radicals by introducing a modified expression for ν_0 as[34]

$$\nu_{0,eff}(T) = \nu_0 - \frac{\omega_0}{\exp(\theta_0/T) - 1} \quad (9)$$

Ikeda et al. later on also tested this method for the simulation of the T-dependent σ values of benzyl radicals.[36] This modification introduced an asymmetry and T-dependent shift of the Gaussian-type spectrum with the four quantities σ_{max}, ν_0, $\Delta\nu_0$, and θ_0 as fitting parameters. For the spectrum of CH_2I_2 in the 330−400 nm range, we considered only three relevant Gaussian peaks corresponding to wavelengths of 247, 283, and 313 nm. Experimental data at 300 and 1400 K were taken from the shock wave experimental work of Henning et al.[31] and are shown in Figure 4A. Additional experimental data of a more detailed T dependence for $\sigma(CH_2I_2)$ at 400 nm are shown in the inset.[22,31] In the modified Sulzer−Wieland formalism of eqs 8 and 9, we were able to simultaneously fit the three aforementioned experimental data sets in Figure 4A with the parameters σ_{max}, $\Delta\nu_0$, and θ_0. The best global fit of the experimental data was reached when we used values of $\sigma_{max} = 1.9$, 4.0, and 2.9×10^{-18} cm^2 molecule^{-1}; $\Delta\nu_0 = 1400$, 2000, and 2300 cm^{-1}; and $\theta_0 = 432$, 432, and 576 K for the 247, 283, and 313 nm peaks, respectively: they are of similar magnitude as those found by Astholz et al.[34] The resulting simulations are shown in Figure 4A as lines at 300 and 4000 K in the main Figure, and a T-dependent $\sigma(CH_2I_2)$ at 400 nm in the inset. In Figure 5A, we also plot T-dependent $\sigma(CH_2I_2)$ at other wavelengths in the 330−400 nm region.

In a similar way, we determined the T dependence of the absorption cross section, σ, of the CH_2I radical. Experimental data from Sehested et al. at 300 K[12] and our data at 313 and ∼3400 K were fitted using the modified Sulzer−Wieland formalism. One additional wide Gaussian peak at 230 nm had to be included in addition to the two peaks at 280 and 338 nm, because the experimental data from Sehested et al. contain a broad absorption pedestal extending from ∼230 nm to longer wavelengths. The origin of this broad background is not clear. Figure 4B shows the resulting simulation of T dependence of $\sigma(CH_2I)$ at 300, 1500, and 3400 K. The following parameters were obtained for best agreement with the experiments: $\sigma_{max} = 7.2$, 6.8, and 4.7×10^{-18} molecule^{-1} cm^2; $\Delta\nu_0 = 6544$, 1456, and 675 cm^{-1}; and $\theta_0 = 91$, 1605, and 211 K for the 230, 280, and 338 nm peaks, respectively. The resulting T-dependent $\sigma(\lambda,T)$ of CH_2I radicals in the wavelength range 330−400 nm are plotted in Figure 5B. Considering the error range ∼20−30% in our experimental values of $\sigma(CH_2I^*)$ and $\sigma(CH_2I)$, the simulation results of the Sulzer−Wieland fit in Figure 5B contain ∼10−15% uncertainty.

We hope that our simulation results in Figure 5 will be useful in the interpretation of ultrafast transient absorption experiments on the dynamics of the CH_2I radical after CH_2I_2 photolysis and also for future kinetic studies of these types of systems, for example, in terms of giving reasonable estimates and error ranges for $\sigma(CH_2I)$ and $\sigma(CH_2I_2)$, when one does not know the exact temperature of these species.

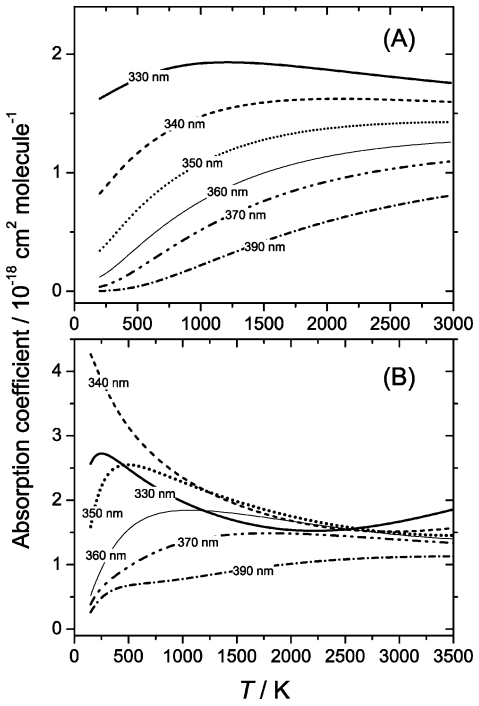

Figure 5. Temperature dependence of the absorption coefficients of CH_2I_2 (A) and CH_2I (B) estimated from a modified Sulzer−Wieland formalism (see text). Thick solid line, at 330 nm; dashed line, at 340 nm; dotted line, at 350 nm; thin solid line, at 360 nm; dash−dot−dotted line, at 370 nm; dash−dotted line, at 390 nm.

3.4. Master Equation Simulations. To characterize the deactivation of CH_2I^* by CH_2I_2 in more detail, we carried out additional master equation simulations of its stepwise collisional relaxation. Time-resolved absorption profiles of the CH_2I radicals were extracted from the kinetic fitting procedure and compared with the results of the aforementioned analysis to obtain information about the average energy transferred per collision, $\langle\Delta E\rangle$. In addition, the master equation approach allowed us to estimate how sensitive the absorption profiles were to the shape of the CH_2I^* population distribution.

For the simulations, we employed a realistic initial CH_2I^* distribution based on the ion imaging results of Xu et al. after laser excitation of CH_2I_2 around 304 nm.[9] In these experiments, they identified two major dissociation pathways leading to $CH_2I + I(^2P_{3/2})$ (termed G1 and G2 in their paper), which occur with roughly equal probabilities, forming highly internally excited CH_2I molecules with energies of about 13 200 and 11 590 cm^{-1}, respectively. A third major channel (termed G*) leads to $CH_2I + I^*(^2P_{1/2})$, where the CH_2I is formed with 5670 cm^{-1} excess energy. On the basis of their translational energy distributions, we estimate the widths of the G1, G2, and G* populations to be on the order of 1100, 1600, and 1000 cm^{-1}, respectively. The shape of each component can be well described by a Gaussian function. We also have to consider the longer excitation wavelength (308 nm) in our experiments, which reduces the starting energy by about 430 cm^{-1}, leading to average internal energies of 12 770, 11 170, and 5250 cm^{-1} for G1, G2, and G*, respectively. Following Baugchum and Leone, approximately 75% of the CH_2I_2 precursors dissociate, forming ground state iodine atoms; that is, 37.5% appear in each of the components G1 and G2, whereas 25% appear in the channel,

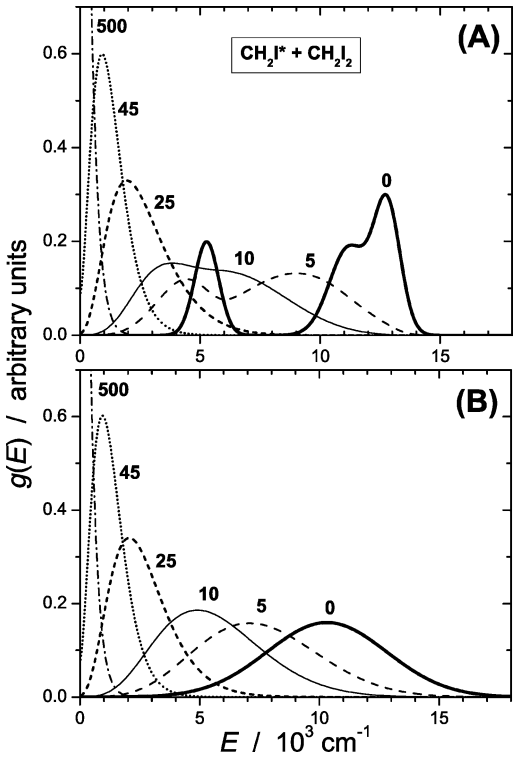

Figure 6. Master equation simulations of the collisional deactivation of a highly vibrationally excited CH_2I^* radical population distribution in a CH_2I_2 bath: (A) using a trimodal start distribution, as present in the experiments; (B) with an initial monomodal distribution having the same average energy as the trimodal distribution in part A. The numbers denote the number of collisions experienced by the respective population distribution. For details, see the text.

forming spin−orbit excited iodine atoms.[3] The resulting initial CH_2I^* distribution is shown in Figure 6A as a thick solid line ("0" collisions). It is clearly trimodal. The low-energy component is due to the G* population (I* channel), and the coalescing high-energy components correspond to the G1 and G2 populations (I channel). The average energy of the whole distribution is about 10 300 cm^{-1}.

The evolution of this initial CH_2I^* population under the influence of collisions was investigated using a master equation approach, as described in detail previously.[20] Briefly, one sets up the master equation for the collision processes as

$$\frac{dg(E,t)}{d(Z[M]t)} = \int_0^\infty [P(E,E')\, g(E',t) - P(E',E)\, g(E,t)]\, dE' \quad (10)$$

where $g(E,t)$ is the time-dependent vibrational CH_2I population at energy E. Z denotes the collision number. $P(E',E)$ represents the collisional transition probability density function, which describes the probability for a collision of CH_2I^* starting at energy E to finish at energy E'. Recent experiments using KCSI detection for several polyatomic systems have shown that $P(E',E)$ can be well described by the expression[20,37]

$$P(E',E) = \frac{1}{c(E)} \exp\left[-\left(\frac{E-E'}{C_0 + C_1 E}\right)^Y\right] \quad \text{with} \quad E' \le E \quad (11)$$

which is of monoexponential type with flexible shape determined by the parametric exponent Y in the argument. The denominator $C_0 + C_1E$, which has typically a linear dependence on energy, describes the width of the energy transfer probability and is thus related to the efficiency of the collisions. $c(E)$ is a normalization constant. The upward branch ($E' > E$) of $P(E',E)$ is given by detailed balance. Because the shape of the transition probability function for $CH_2I^* + CH_2I_2$ collisions is not known, we use a standard monoexponential form with $Y = 1$ as the best compromise between the values <1 normally found for smaller colliders such as rare gases and values >1 for efficient colliders such as larger alkanes.[20,37] Solution of the master equation (eq 10) provides the time evolution of the population, $g(E,t)$. The parameters C_0 and C_1 were optimized to achieve the best fit to the time-resolved CH_2I^* absorption profiles. For this, the resulting $g(E,t)$ were convolved with the energy-dependent absorption cross sections, $\sigma(E)$, from the Sulzer−Wieland formalism presented in section 3.3 to obtain a calculated population-averaged transient absorption signal, $\langle\sigma(t)\rangle$, via

$$\langle\sigma(t)\rangle = \int_0^\infty g(E,t)\, \sigma(E)\, dE \quad (12)$$

where the conversion between energy and temperature in the Sulzer−Wieland cross section can be achieved using the canonical partition function of CH_2I. During the course of this modeling, it was found that a strongly energy-dependent denominator with $C_0 = 20$ cm^{-1} and $C_1 = 8 \times 10^{-2}$ in eq 11 gave the best fit to the absorption time profiles.

The temporal evolution of the CH_2I^* population due to collisional deactivation by CH_2I_2 is shown in Figure 6A, where each number denotes the number of collisions experienced by the respective population distribution. It can be clearly seen that the distribution broadens substantially already after a few collisions. In addition, the trimodal character quickly smoothes out. With an increasing number of collisions, the distribution narrows, and after 500 collisions, the thermal CH_2I Boltzmann distribution has already been reached. To assess the influence of the shape of the initial distribution on the deactivation, we also carried out calculations with a monomodal distribution (Gaussian shape with a width of 5000 cm^{-1}), which had the same average energy as the trimodal start distribution present in the experiments. The results are shown in Figure 6B. In the early stage of the deactivation, the distributions differ considerably, whereas later on they look very similar.

Interestingly, the resulting absorption profiles generated from the two different master equation simulations using eq 12 are nevertheless almost indistinguishable. An example for the probe wavelength 390 nm is shown in Figure 7, where the dashed and dotted curves are the fits originating from the simulations employing the trimodal and monomodal distribution, respectively. We extracted the solid curve from the kinetic modeling performed in Figure 2 at 390 nm without the contribution of the loss of cold CH_2I radicals by reactions, that is, considering only processes 2 and 3. It is very well reproduced by both fits. Figure 7 clearly demonstrates that the time-resolved UV absorption profiles are completely insensitive to the exact shape of the distribution and are only sensitive to the average energy, $\langle E\rangle$, of the excited molecules. This is in agreement with findings of KCSI experiments on the collisional energy transfer of highly vibrationally excited toluene and azulene molecules by Lenzer, Luther, and co-workers, which show that UV absorption (and also IR emission) time traces cannot give information on the shape of the underlying population distribution, only on the change of the average energy of the excited molecules with time.[20,37] Our result also agrees very well with earlier studies of Hippler and co-workers, which showed that UV absorption coefficients of distributions with the same average energy obtained after either laser excitation (microcanonical) or heating in shock waves (canonical) are practically identical, although

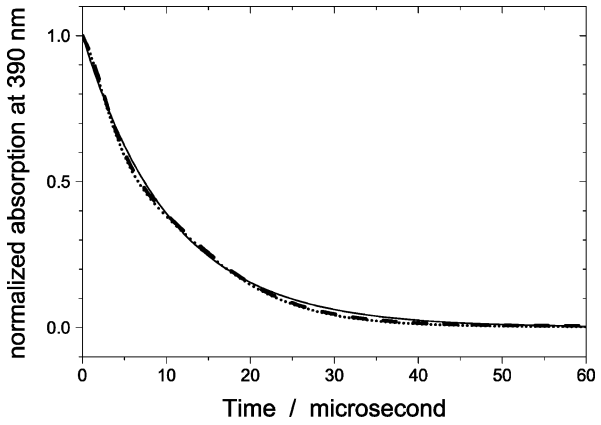

Figure 7. Fitted absorption profile for CH_2I^* collisional deactivation by CH_2I_2 at a probe wavelength of 390 nm. Solid line, experimental trace extracted from the kinetic modeling. Dashed and dotted lines, fits on the basis of eq 12 originating from the master equation simulations employing the trimodal and monomodal start distribution, respectively, as shown in Figure 6. Note that the simulated absorption profiles are essentially identical, although the shape of the transient $g(E,t)$ distributions is very different, especially after a few collisions (compare Figure 6).

the underlying population distributions differ significantly in shape.[38] For our current analysis of CH_2I^* relaxation, this implies that uncertainties in the initial distribution will have no influence on the kinetic modeling, as long as the temporal evolution of the average CH_2I^* vibrational energy, $\langle E(t)\rangle$, is correctly described by the model. In addition, this validates the approach taken in our simplified kinetic modeling, where the deactivation was described in terms of a simple superposition of contributions from hot CH_2I^* and cold CH_2I radicals, each having their own characteristic absorption cross section. Varying concentrations of these two species during the collision cascade will then result in a time-dependent change in absorption, which adequately describes the changing amount of internal energy during the deactivation.

Finally, we would like to comment briefly on the resulting energy transfer parameters we obtain from our master equation simulations. Using our best fit parameters $C_0 = 20$ cm^{-1} and $C_1 = 8 \times 10^{-2}$ in eq 11, and the hard-sphere collision number, Z, used by Baugchum and Leone,[3] average energies transferred per collision can be determined via

$$\langle \Delta E(E)\rangle = \int_0^{\infty} (E' - E)\, P(E',E)\, \mathrm{d}E \qquad (13)$$

This way, we obtain $\langle \Delta E\rangle$ values of -320 cm^{-1} (at $E = 5670$ cm^{-1}) and -800 cm^{-1} (at $E = 11\,970$ cm^{-1}), which can be compared with the -1250 and -1900 cm^{-1} values estimated by Baughcum and Leone at these energies.[3] The deactivation we observe is therefore by a factor of 2.5−4 slower than suggested by Leone's results. However, our values are in reasonable agreement with direct measurements for other systems with a similar "size" of the excited species. For instance, Hippler and co-workers studied the collisional deactivation of highly vibrationally excited CF_3I with *n*-octane using the time-resolved UV absorption technique. They found $\langle \Delta E\rangle$ values of -250 and -700 cm^{-1} at the energies mentioned above, in reasonable agreement with the current study.[39] Values for a smaller collider like CH_2I_2 will be expected to lie in the same range or probably even slightly smaller, because efficient V−V energy transfer is expected to be less efficient due to the smaller number of low-frequency acceptor modes in a smaller bath gas molecule.[20,37] This argument gives further support to our smaller value. We also do not expect any "anomalous" effects due to the open-shell structure of CH_2I, because, for example, studies on toluene and benzyl deactivation show very similar energy transfer behavior.[20,40] Part of the disagreement between Leone's and our values might be also due to the well-known fact that IR emission studies of collisional energy transfer can show deviations from the "exact" $\langle \Delta E\rangle$ values within a factor of 5, due to uncertainties in the calibration curve relating the infrared emission and the average energy of the excited molecules, as recently demonstrated in KCSI studies of systems such as toluene and azulene.[19,20,37] So far, such a large discrepancy has not been observed in comparison with results from the UV absorption technique.

4. Conclusions

We observed transient UV absorption spectra following 308 nm laser photolysis of CH_2I_2 in the gas phase. The spectra were found to be a mixture of hot and cold CH_2I radicals and parent CH_2I_2 in the early time range up to a few microseconds. From the simulation of time-resolved absorption signals between 330 and 400 nm, we further estimated the transient absorption spectra of hot and cold CH_2I radicals. The wavelength and temperature dependence of the absorption coefficients of CH_2I radicals and CH_2I_2 molecules have been simulated using a modified Sulzer−Wieland formalism. Our master equation simulations have shown that the collisional energy transfer efficiency in CH_2I^* + CH_2I_2 collisions is in reasonable agreement with earlier direct studies of the collisional relaxation of related systems, like CF_3I^* + *n*-octane. In addition, our simulations show that the measured UV absorption signals are insensitive to the actual shape of the vibrational population distribution of hot CH_2I^* radicals.

In the photodissociation dynamics of CH_2I_2 in dense fluids, there has been a debate on the assignment of the transient absorption spectrum in the 330−450 nm region, in particular for delay times of a few picoseconds (see, e.g., refs 13−16). Grimm et al.[16] suggested that the transient absorption in this region could be the result of contributions from electronically excited CH_2I_2, hot CH_2I^* radicals, and contact charge transfer pairs of iodine atoms and CH_2I radicals. Our results partly support this idea in the aspect that the absorption spectra of hot CH_2I^* radicals and vibrationally excited $CH_2I_2^*$ molecules would extend into the relevant spectral region at sufficiently high excess energies as they are attained after UV photolysis of CH_2I_2.

Acknowledgment. Financial support by the Alexander von Humboldt Foundation within the "Sofja Kovalevskaja Program" as well as helpful discussions with J. Zerbs, P. Wagener, K. Luther, and J. Troe are gratefully acknowledged.

References and Notes

(1) Kawasaki, M.; Lee, S. J.; Bersohn, R. *J. Chem. Phys.* **1975**, *63*, 809.

(2) Kroger, R. P.; Demou, P. C.; Riley, S. J. *J. Chem. Phys.* **1976**, *65*, 1823.

(3) Baughcum, S. L.; Leone, S. R. *J. Chem. Phys.* **1980**, *72*, 6531.

(4) Koffend, J. B.; Leone, S. R. *Chem. Phys. Lett.* **1981**, *81*, 136.

(5) Cain, S. R.; Hoffmann, R.; Grant, E. R. *J. Phys. Chem.* **1981**, *85*, 5.

(6) Schmitt, G.; Comes, F. J. *J. Photochem.* **1980**, *14*, 107.

(7) Hunter, T. F.; Kristjansson, K. S. *J. Chem. Soc., Faraday Trans. 2* **1982**, *78*, 2067.

(8) Zhang, J.; Heller, E. J.; Huber, D.; Imre, D. G.; Tannor, D. *J. Chem. Phys.* **1988**, *89*, 3602.

(9) Xu, H.; Guo, Y.; Liu, S.; Ma, X.; Dai, D.; Sha, G. *J. Chem. Phys.* **2002**, *117*, 5722.

(10) Jung, K.-W.; Ahmadi, T. S.; El-Sayed, M. A. *Bull. Korean Chem. Soc.* **1997**, *18*, 1274.
(11) Hippler, H.; Troe, J.; Wendelken, H. J. *J. Chem. Phys.* **1983**, *78*, 5351.
(12) Sehested, J.; Ellermann, T.; Nielsen, O. J. *Int. J. Chem. Kinet.* **1994**, *26*, 259.
(13) Schwartz, B. J.; King, J. C.; Zhang, J. Z.; Harris, C. B. *Chem. Phys. Lett.* **1993**, *203*, 503.
(14) Saitow, K.; Naitoh, Y.; Tominaga, K.; Yoshihara, K. *Chem. Phys. Lett.* **1996**, *262*, 621.
(15) Tarnovsky, A. N.; Alvarez, J.; Yartsev, A. P.; Sundström, V.; Åkesson, E. *Chem. Phys. Lett.* **1999**, *312*, 121.
(16) Grimm, C.; Kling, G.; Schroeder, J.; Troe, J.; Zerbs, J. *Isr. J. Chem.* **2003**, *43*, 305.
(17) Tarnovsky, A. N.; Sundström, V.; Åkesson, E.; Pascher, T. *J. Phys. Chem. A* **2004**, *108*, 237.
(18) Odelius, M.; Kadi, M.; Davidsson, J.; Tarnovsky, A. N. *J. Chem. Phys.* **2004**, *121*, 2208.
(19) Grigoleit, U.; Lenzer, T.; Luther, K.; Mützel, M.; Takahara, A. *Phys. Chem. Chem. Phys.* **2001**, *3*, 2191.
(20) Lenzer, T.; Luther, K.; Reihs, K.; Symonds, A. C. *J. Chem. Phys.* **2000**, *112*, 4090.
(21) Bingemann, D.; King, A. M.; Crim, F. F. *J. Chem. Phys.* **2000**, *113*, 5018.
(22) Charvat, A.; Assmann, J.; Abel, B.; Schwarzer, D.; Henning, K.; Luther, K.; Troe, J. *Phys. Chem. Chem. Phys.* **2001**, *3*, 2230.
(23) Charvat, A.; Assmann, J.; Abel, B.; Schwarzer, D. *J. Phys. Chem. A* **2001**, *105*, 5071.
(24) Sekiguchi, K.; Shimojima, A.; Kajimoto, O. *Chem. Phys. Lett.* **2002**, *356*, 84.
(25) Sekiguchi, K.; Shimojima, A.; Kajimoto, O. *Chem. Phys. Lett.* **2003**, *370*, 303.
(26) Elles, C. G.; Bingemann, D.; Heckscher, M. M.; Crim, F. F. *J. Chem. Phys.* **2003**, *118*, 5587.
(27) Hippler, H.; Luther, K.; Troe, J. *Ber. Bunsen-Ges. Phys. Chem.* **1973**, *77*, 1104.
(28) Rasmusson, M.; Tarnovsky, A. N.; Pascher, T.; Sundström, V.; Åkesson, E. *J. Phys. Chem. A* **2002**, *106*, 7090.
(29) Furuyama, S.; Golden, D. M.; Benson, S. W. *J. Phys. Chem.* **1968**, *72*, 4713.
(30) Furuyama, S.; Golden, D. M.; Benson, S. W. *J. Am. Chem. Soc.* **1969**, *91*, 7564.
(31) Henning, K. Ph.D. Thesis, University of Göttingen, 2000.
(32) Sulzer, P.; Wieland, K. *Helv. Phys. Acta* **1952**, *25*, 653.
(33) Troe, J.; Wieters, W. *J. Chem. Phys.* **1979**, *71*, 3931.
(34) Astholz, D. C.; Brouwer, L.; Troe, J. *Ber. Bunsen-Ges. Phys. Chem.* **1981**, *85*, 559.
(35) Brouwer, L.; Troe, J. *Chem. Phys. Lett.* **1981**, *82*, 1.
(36) Ikeda, N.; Nakashima, N.; Yoshihara, K. *J. Phys. Chem.* **1984**, *88*, 5803.
(37) Hold, U.; Lenzer, T.; Luther, K.; Symonds, A. C. *J. Chem. Phys.* **2003**, *119*, 11192.
(38) Brouwer, L.; Hippler, H.; Lindemann, L.; Troe, J. *J. Phys. Chem.* **1985**, *89*, 4608.
(39) Abel, B.; Herzog, B.; Hippler, H.; Troe, J. *J. Chem. Phys.* **1989**, *91*, 900.
(40) Damm, M.; Deckert, F.; Hippler, H. *Ber. Bunsen-Ges. Phys. Chem.* **1997**, *101*, 1901.